Electronic Supporting Information for

A Well-Defined Terminal Vanadium(III) Oxo Complex

Amanda E. King,[a,b]‡ Michael Nippe[a,b]‡ Mihail Atanasov,*[c,g] Teera Chantarojsiri,[a] Curtis A. Wray,[a] Eckhard Bill,[c] Frank Neese,*[c] Jeffrey R. Long,*[a,d] and Christopher J. Chang*[a,b,e,f]

[a]Department of Chemistry, University of California, Berkeley, USA; [b]Chemical Sciences Division, Lawrence Berkeley National Laboratory, Berkeley, USA; [d]Materials Sciences Division, Lawrence Berkeley National Laboratory, Berkeley, USA; [e]Department of Molecular and Cell Biology, University of California, Berkeley, USA; [f]Howard Hughes Medical Institute, University of California, Berkeley, USA

[c]Max-Planck Institut für Chemische Energiekonversion, Mülheim an der Ruhr, D-45470, Germany

[g]Institute of General and Inorganic Chemistry, Bulgarian Academy of Sciences, Acad. Georgi Bontchev Str 11, 1113 Sofia, Bulgaria

chrischang@berkeley.edu; jrlong@berkeley.edu; frank.neese@cec.mpg.de; mihail.atanasov@cec.mpg.de

‡These authors contributed equally.

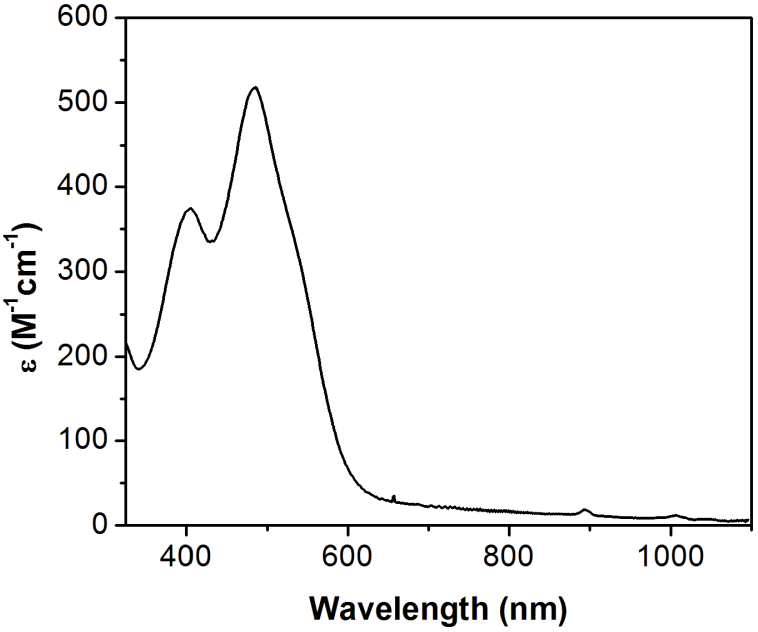

Figure S1. UV/vis spectrum of **1** in CH_3CN.

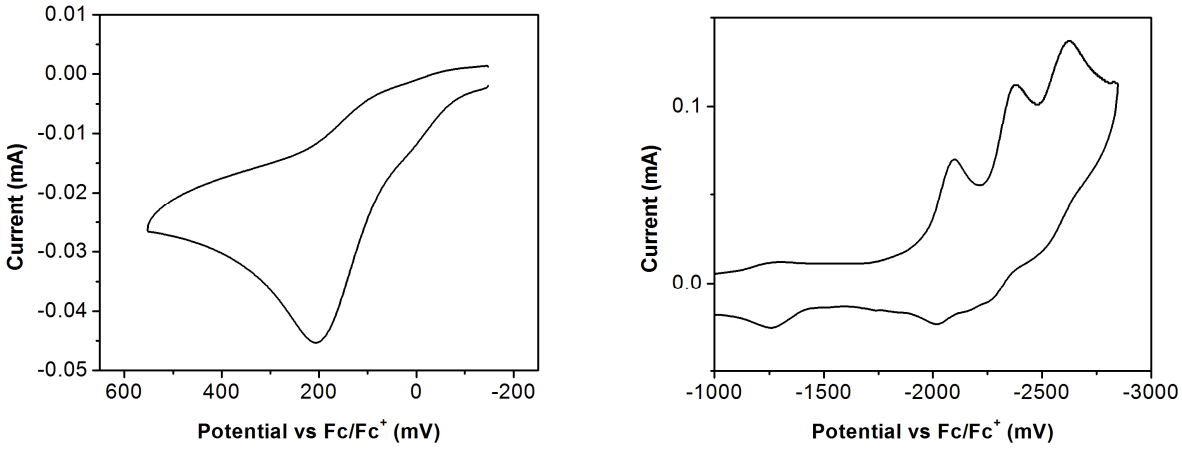

Figure S2. Anodic (left) and cathodic (right) scans of **1** in CH_3CN.

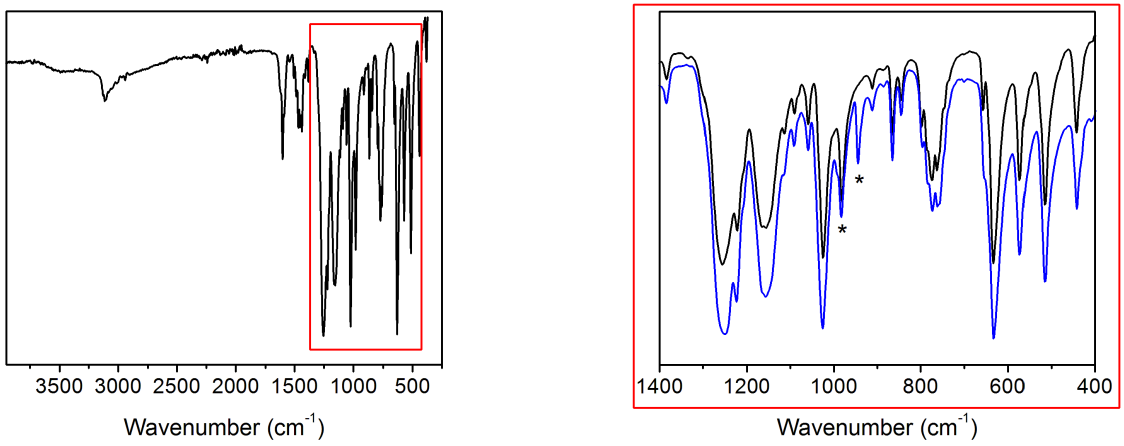

Figure S3. Full (left) and insert (right) IR spectra of **2** and ^{18}O labeled **2**. In the inset spectra, the black trace corresponds to ^{16}O-labeled **2** while the blue trace corresponds to ^{18}O-labeled **2**. The presence of unlabeled **2** is due to the introduction of advantageous air during the synthesis of labeled **2**.

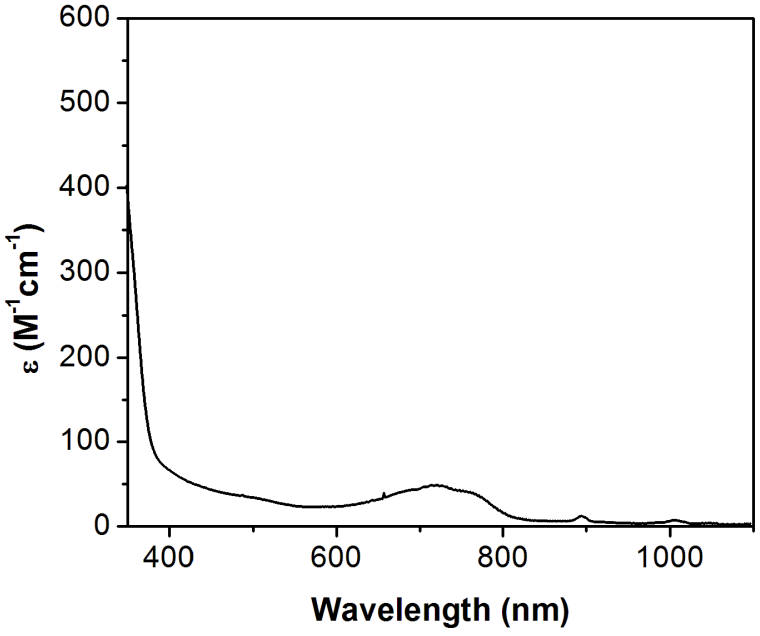

Figure S4. UV/vis spectrum of **2** in CH_3CN.

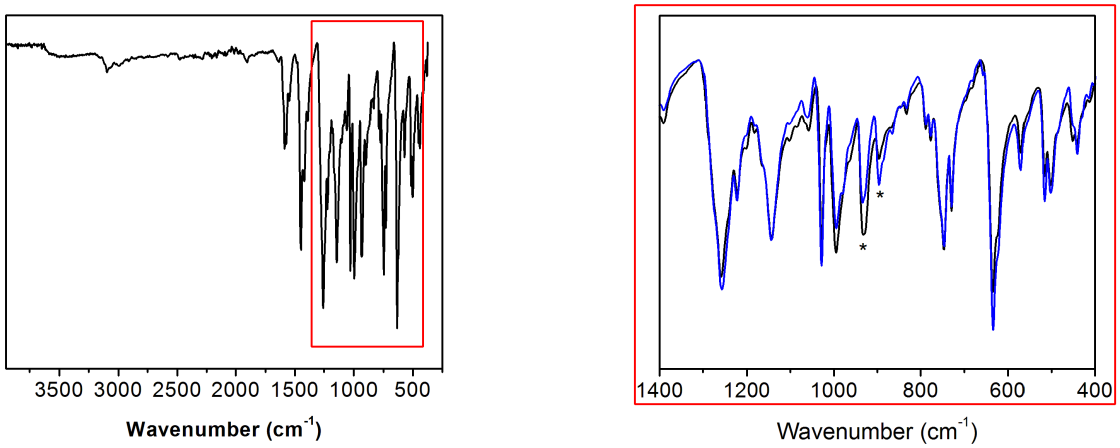

Figure S5. Full (left) and insert (right) IR spectra of **3** and ^{18}O labeled **3**. In the inset spectra, the black trace corresponds to ^{16}O-labeled **3** while the blue trace corresponds to ^{18}O-labeled **3**. The band at 895 cm^{-1} in labeled **3** overlaps with a weak band present in unlabeled **3**. The band at 929 cm^{-1} in labeled **3** results from the isotopic impurity present ^{18}O-labeled **2**.

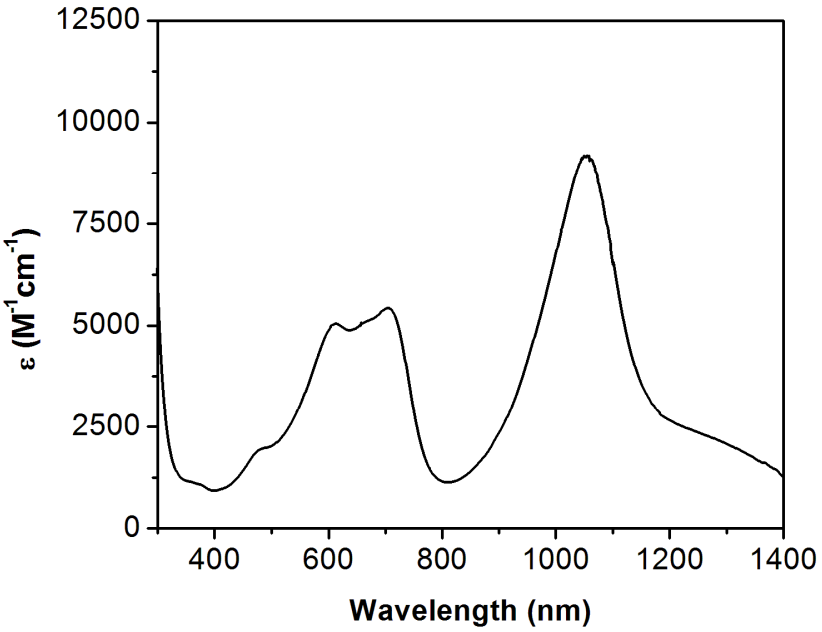

Figure S6. UV/vis/NIR spectrum of **3** in CH_3CN.

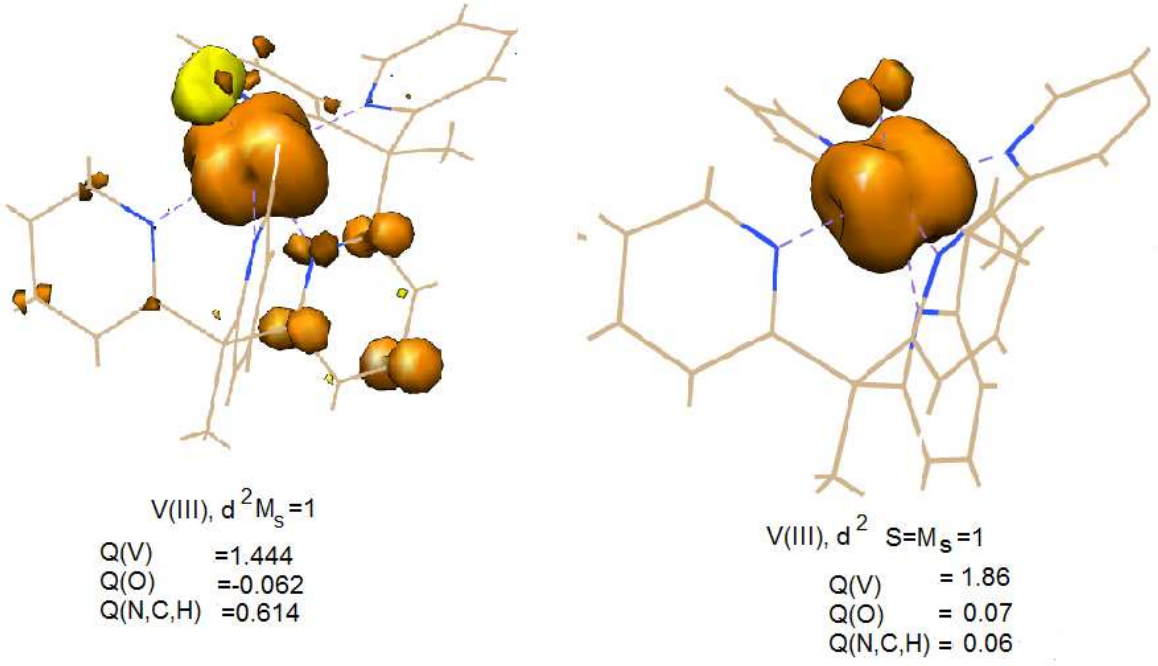

Figure S7. Ground state spin-density plots from B3LYP (left) and CASSCF (right) calculations of **3** with the B3LYP optimized geometry; contour plots are given for values of the spin-density of +0.005 (orange, B3LYP, CASSCF) and -0.005(yellow, B3LYP); Löwdin spin-populations Q at the V, O and the total of the N,C,H sites are shown; both B3LYP and NEVPT2 yield triplet excited states with energies of 5.30 kcal/mole (B3LYP), 5.91 kcal/mole (NEVPT2) higher than the low-spin ground states.

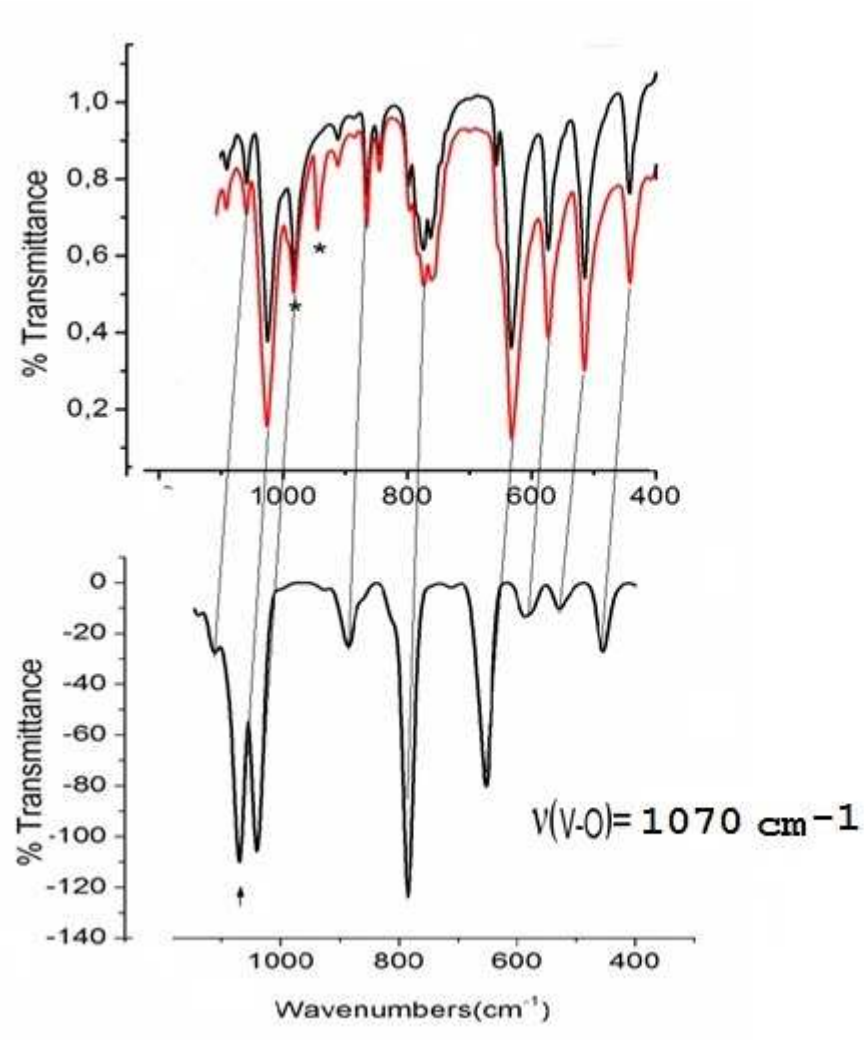

Figure S8. Experimental (top) versus the theoretically computed (bottom, based on a B3LYP(def2-TZVP basis S =1/2 DFT optimized geometry) IR spectrum of **2**.

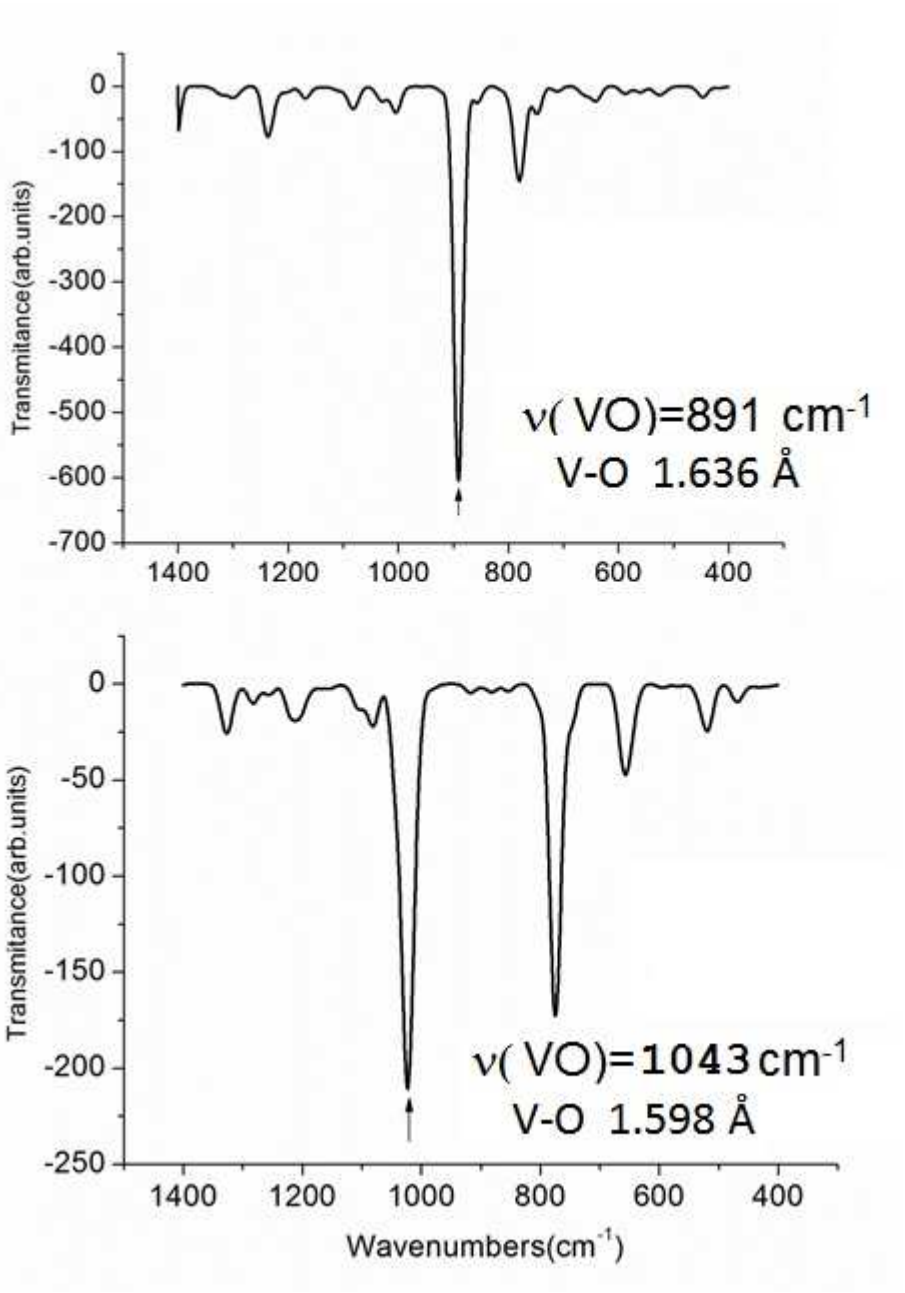

Figure S9. Theoretical IR spectra of **3** (DFT/B3LYP optimized geometries for S = 1 (top) and S = 0 (bottom)). The correlation between the computed V-O vibrational frequency with the V-O equilibrium bond lengths in the two spin forms of the complex is indicated.

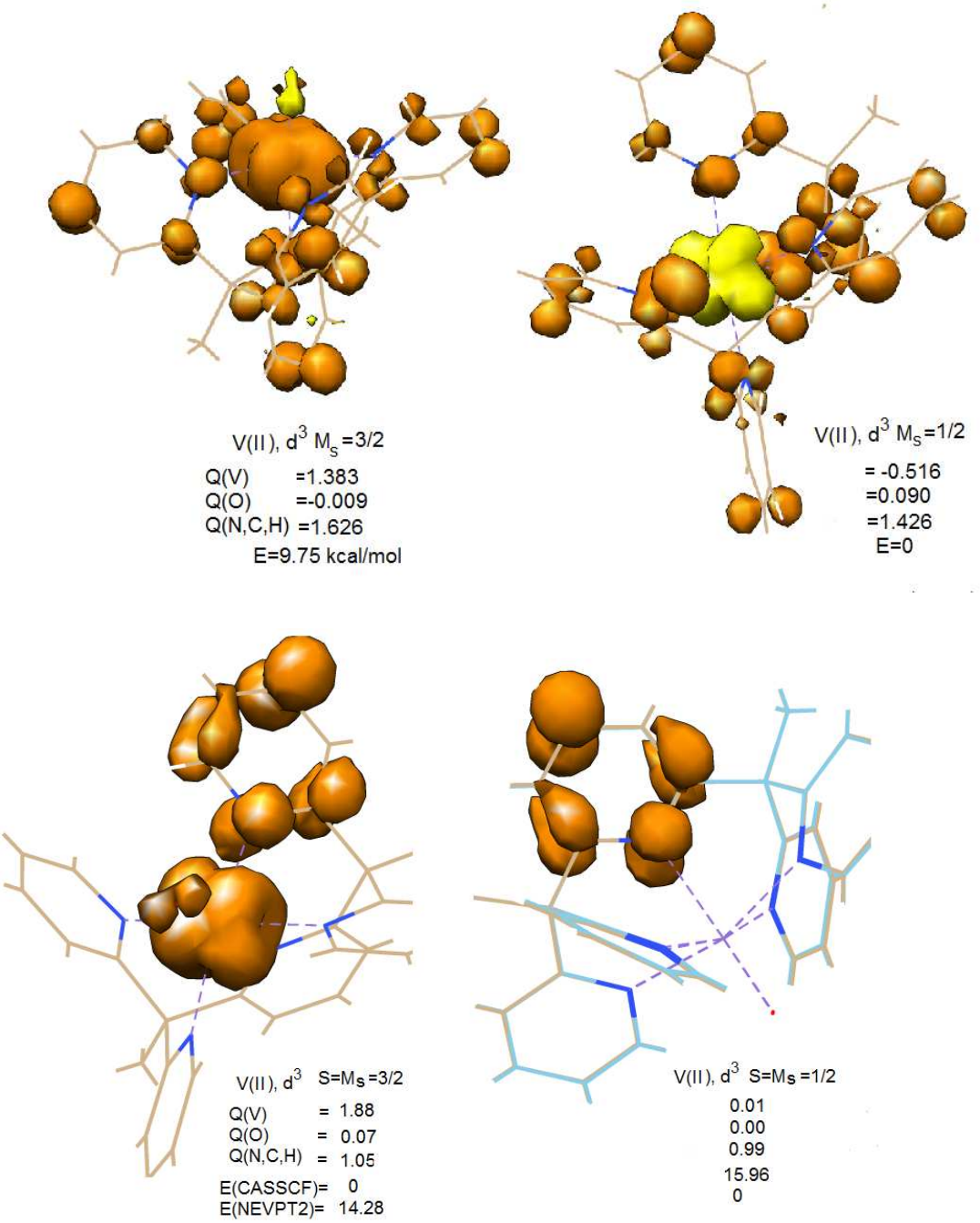

Figure S10. Ground state spin-density plots from B3LYP (top) and CASSCF (bottom) calculations of neutral **4** with the B3LYP optimized geometry; contour plots are given for values of the spin-density of +0.005 (orange, B3LYP, CASSCF) and -0.005(yellow, B3LYP); Löwdin spin-populations Q at the V, O and the total of the N,C,H sites are shown; The energy of the high-spin form with respect to the low-spin one are is given in kcal/mol.

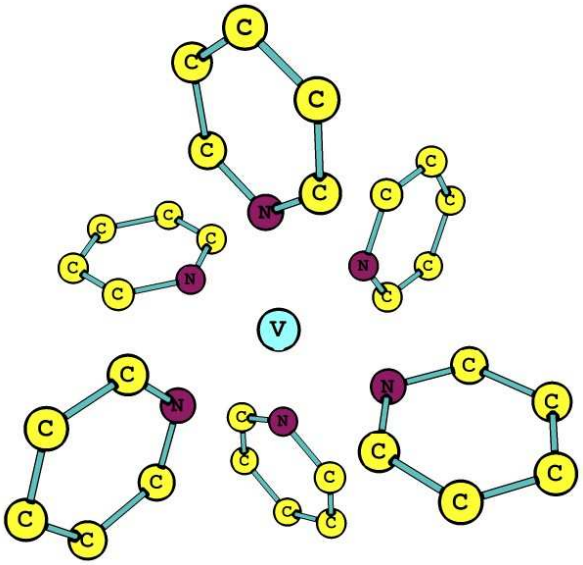

Figure S11. $[V(py)_6]^{n+}$ (n=0,2,3,4) model complexes employed for the exploration of V-N_{py} bond using a best fit of the angular overlap model parameters to the 5x5 ligand field matrices from *ab initio* ligand field calculations.

Table S1. Crystallographic Data.

Compound	**1**	**2**	**3**
Formula	C37 H34 F6 N8 O6 S2 V	C68 H59 F12 N13 O14 S4 V2	C30 H25 F3 N5 O4 S V
Crystal system	Monoclinic	Orthorhombic	Monoclinic
Space group	*P 21/n*	*Cmc21*	*P 21/c*
a, Å	12.5042(7)	14.8802(5)	8.7910(5)
b, Å	15.8420(9)	22.0171(7)	20.233(1)
c, Å	20.147(1)	21.9728(7)	15.2867(8)
α, °	90	90	90
β, °	90.8446(9)	90	90.280(3)
γ, °	90	90	90
V, Å^3	3990.5(7)	7198.7(4)	2719.0(7)
Z	4	4	4
ρ, Mg m^{-3}	1.524	1.606	1.611
R1[a], *w*R2[b] ($I > 2\sigma(I)$)	0.0502, 0.1267	0.0263, 0.0670	0.0942, 0.1980
R1[a], *w*R2[b] (all data)	0.0688, 0.1424	0.0272, 0.0679	0.1247, 0.2101

[a]$R1 = 3||F_o| - |F_c||/3|F_o|$. [b]$wR2 = [3[w(F_o^2 - F_c^2)^2]/3[w(F_o^2)^2]]^{½}$, $w = 1/\sigma^2(F_o^2) + (aP)^2 + bP$, where $P = [\max(0 \text{ or } F_o^2) + 2(F_c^2)]/3$.

Table S2. Energies of electronic transitions for **2** and $[V(py)_6]^{4+}$.[a]

	2		$[V(py)_6]^{4+}$	
	CASSCF	NEVPT2	CASSCF	NEVPT2
$^2B_2(d_{xy})$	0	0	0	0
$^2E(d_{xz},d_{yz})$	12709	17509	796	918
	13157	17948	995	1095
$^2B_1(d_{x2-y2})$	17269	21886	20426	25673
$^2A_1(d_{z2})$	34695	40629	20505	25756

[a] based on a B3LYP(def2-TZVP basis) M_s=1/2 DFT optimized geometries.

Table S3. X-ray structure and Löwdin spin-populations (Q) and DFT, B3LYP(BP86) optimized metal-ligand bond distances of complex **3**.

	exp.	B3LYP(BP86) *S* = 1	B3LYP(BP86) *S* = 0
E(kcal/mol)	-	5.26(7.66)	0(0)
Q(V)	-	1.444(1.290)	-
Q(O)	-	-0.062(-0.020)	-
Q(N,C,H)	-	0.614(0.730)	-
R(V-O)	1.621[4]	1.635(1.658)	1.598(1.617)
R(V-N_{ax})	2.266[5]	2.206(2.205)	2.337(2.307)
R(V-N_{eq})	2.103[5]	2.151(2.123)	2.124(2.095)
	2.079[5]	2.149(2.122)	2.122(2.095)
	2.106[5]	2.152(2.123)	2.125(2.095)
	2.085[5]	2.150(2.123)	2.125(2.095)

Table S4. Non-relativistic energies of electronic multiplets of **3** from state average CASSCF/NEVPT2 calculations.

Electronic term $C_{4v}[O_h]$	CASSCF	NEVPT2
$^3E[^3T_1(1)]$	0 884	0 795
$^3A_2[^3T_1(1)]$	8090	9457
$^3B_2[^3T_2]$	15096	18224
$^3E[^3T_2]$	15964 18174	18323 18431
$^3A_2[^3A_2]$	18589	19148
$^3A_2[^3T_1(2)]$	33528	40187
$^3E[^3T_1(2)]$	37613 39348	38323 38483

[a] active space : 2 electrons on the five 3d orbitals, CAS(2,5), state averaging over the 10 S=1 and 15 S=0 electronic multiplets of the d^2 configuration; calculations are based on the B3LYP optimized geometry of **3**; listed energies are in cm^{-1}.

Table S5. Löwdin spin-populations (Q) and optimized metal-ligand bond distances from B3LYP and BP86 DFT geometry optimizations of **4**.

	B3LYP		BP86	
	M_s=3/2	M_s=1/2	M_s=3/2	M_s=1/2
E(kcal/mol)	9.86	0	9.91	0
Q(V) Q(O) Q(N,C,H)	1.363 -0.010 1.647	-0.510 0.089 1.421	1.362 0.071 1.567	0.210 0.042 0.748
R(V-O)	1.643	1.614	1.695	1.652
R(V-N_{ax})	2.209	2.238	2.196	2.212
R(V-N_{eq})	2.128 2.130 2.131 2.127	2.112 2.109 2.110 2.106	2.107 2.107 2.106 2.107	2.082 2.082 2.083 2.083

Table S6. Equilibrium V-N bond distances, relative energies and Löwdin spin-populations (Q) for $[V(py)_6]$ model complexes [a] with variable vanadium oxidation states from spin-unrestricted B3LYP/def2-TZVP DFT geometry optimizations.

Complex	$[V^{IV}(py)_6]^{4+}$	$[V^{III}(py)_6]^{3+}$		$[V^{II}(py)_6]^{2+}$		$[V(py)_6]^{0}$	
M_s	1/2	1	0	3/2	1/2	5/2	1/2
Rel.energy[b]	-	0	39.62	0	19.60	3.24	0
R(V-N)[b]	2.155	2.200	2.204	2.300	2.286	2.248	2.248
Q(V)	1.177	2.016	-	2.890	0.980	2.773	2.656
Q(N)	-0.121	-0.079	-	-0.059	-0.008	0.472	-0.486
Q(C,H)	-0.056	0.063	-	0.169	0.028	1.754	-1.170

[a] From the listed complexes only $[V^{II}(py)_6]^{2+}$ has been reported to form in the course of the disproportionation reaction: $3V^0(CO)_6 + 6(py) \rightarrow [V^{II}(py)_6]^{2+} + 2[V(CO)_6]^{1-} + 6CO$, see T.G.Richmond, Q.-Z.Shi, W.C.Trogler and F.Basolo, *J. Am. Chem. Soc.* **1984**, 106, 76-80.

[b] Relative energies of the model complexes with alternative spin-ground states are given in kcal/mol with the state of lowest energy as an energy reference; V-N octahedral bond distances are given in Å.

Table S7. Relative energies of the complexes with $S = 1$ and $S = 0$ DFT optimized geometries, Löwdin spin-populations (Q) and selected DFT B3LYP optimized geometry parameters for **5**.

	$S = 1$	$S = 0$
complex	**5**	**5**
E(kcal/mol)	0	24.95
Q(V)	1.949	-
Q(O)	-0.016	-
Q(N,C,H)	0.009	-
R(V-O)/Å	1.825	1.743
$R(V\text{-}N_{ax})$/ Å	2.187	2.198
$R(V\text{-}N_{eq})$[a]/ Å	2.158	2.146
R(O-H)/ Å	0.965	0.961
∠V-O-H/°	125.26	153.72

[a] Average over the four equatorial bond lengths varying in a narrow range of ±0.003 (M_s=0) Å and ±0.009 (M_s=1).

Table S8.Relative energies (in kcal/mol) and Löwdin spin-populations (Q) for the various spin-configurations of the complexes 2, 3 (M_s=1,0) and 4(M_s=1/2, 3/2) from state specific CASSCF calculation of the state with the lowest energy for a given M_s value (active space CAS(2,5); def2-TZVP basis). Calculations were carried out using spin-unrestricted B3LYP optimized geometries for values of M_s=S indicated.[b]

	Q(V)	Q(O)	Q(N,C,H)	Energy[a]	$<S^2>$
V^{IV},M_s=1/2	0.970	0.002	0.028	-	0.750
V^{III},M_s=1	1.864	0.073	0.063	0 [5.91]	0
V^{III},M_s=0	0	0	0	23.56 [0]	0
V^{II},M_s=3/2	1.879	0.070	1.051	0 [14.28]	3.75
V^{II},M_s=1/2	0.012	0.002	0.986	15.96 [0]	0.75

[a] Conversion of the energies (given in kcal/mol in the table) into cm^{-1} can be done multiplying the given entries by 349.77

[b] Energies from NEVPT2 calculations are given in square brackets.

Table S9. Bond distances (in Å) from X-ray data and from DFT, B3LYP and BP86 calculations of **2**.

Parameter	XRD-structure $[V^{III}O(N_{py})_5](OTf)_2$[a]	B3LYP, M_s=0		BP86, M_s=0	
		calc	calc-exp	calc	calc-exp
V-O (Å)	1.595[2]	1.578	-0.017	1.602	0.007
$V\text{-}N_{py,ax}$(Å)	2.228[2]	2.296	0.068	2.285	0.057
$V\text{-}N_{py,eq}$(Å)	2.122[2]	2.146	0.024	2.126	0.004

Table S10. Bond distances (in Å) from X-ray data and from DFT, B3LYP and BP86 calculations of **3**.

Parameter	XRD-structure $[V^{III}O(N_{py})_5](OTf)$[a]	B3LYP, M_s=0		BP86, M_s=0	
		calc	calc-exp	calc	calc-exp
V-O (Å)	1.621[4]	1.598	-0.023	1.617	-0.004
$V\text{-}N_{py,ax}$(Å)	2.266[5]	2.337	0.071	2.307	0.041
$V\text{-}N_{py,eq}$(Å)	2.094[5]	2.124	0.030	2.095	0.001

Table S11. Vanadium,I=7/2 hyperfine coupling parameter A (in units of 10^4 cm^{-1} [a]) for **2** from B3LYP and PBE0 DFT calculations [b] (top) and the decomposition of the total A(TOT) values into Fermi contact (FC), spin-dipolar (SD) and orbital (ORB, spin-orbit) contributions (bottom).

	$A_{x,y}$	A_z	A_{iso}	$\lvert A_{iso,exp} \rvert$
B3LYP	-26.50 -38.80	-132.76	-66.02	79.20
BPE0	-41.15 -52.70	-145.02	-79.62	

	B3LYP			PBE0		
	$A_{x,y}$	A_z	A_{iso}	$A_{x,y}$	A_z	A_{iso}
A(FC)	-61.65	-61.65	-61.65	-75.04	-75.04	-75.04
A(SD)	37.59 26.19	-63.77	0.00	36.46 25.84	-62.30	0.00
A(ORB)	-2.44 -3.34	-7.34	-4.37	-2.57 -3.50	-7.68	-4.58
A(TOT)	-26.50 -38.80	-132.76	-66.02	-41.15 -52.70	-145.02	-79.62
%(ORB)	9 9	6	7	6 7	5	6

[a] Conversion from the given units to MHz are done on division of the listed numbers by 0.333565.

[b] Computations were done with the following input options: def2-TZVP, def2-TZVP/J, ZORA, RIJCOSX, NoFinalGrid, SOMF(1X), TightScf; Diamagnetic corrections A(DIA) are in all cases smaller than $0.001.10^{-4}$, cm^{-1}; Wall times for the B3LYP/PBE0 computations (parallel execution on 8 processors, PAL8) are 8 h 31 min/12 h 35 min with a computational time entirely dominated by SOC orbital part (93 % of the wall time).